The 12th International Symposium on Virtual Reality, Archaeology and Cultural Heritage VAST (2011)
M. Dellepiane, F. Niccolucci, S. Pena Serna, H. Rushmeier, and L. Van Gool (Editors)

Radiometric Characterization of Spectral Imaging for Textual Pigment Identification

Min H. Kim and Holly Rushmeier

Yale University

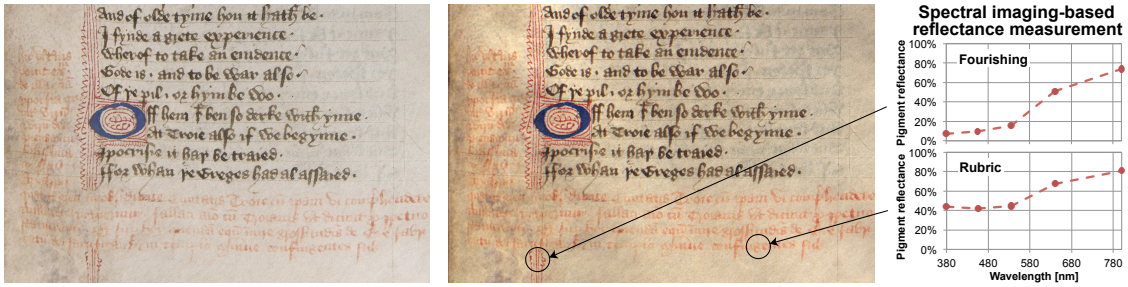

(a) *A commercial RGB camera* **(b)** *Our characterized imaging system to measure radiance*

Figure 1: *Damaged rubric artifacts in a medieval manuscript were captured by (a) an RGB camera and (b) our characterized imager. Our characterized system not only yields more discriminated visual reproduction but measures physically-meaningful radiance at a high accuracy.*

Abstract

Digital imaging of cultural heritage artifacts has become a standard practice. Typically, standard commercial cameras, often commodity rather than scientific grade cameras, are used for this purpose. Commercial cameras are optimized for plausible visual reproduction of a physical scene with respect to trichromatic human vision. However, visual reproduction is just one application of digital images in heritage. In this paper, we discuss the selection and characterization of an alternative imaging system that can be used for the physical analysis of artifacts as well as visually reproducing their appearance. The hardware and method we describe offers a middle ground between the low cost and ease of commodity cameras and the high cost and complexity of hyperspectral imaging systems. We describe the selection of a system, a protocol for characterizing the system and provide a case study using the system in the physical analysis of a medieval manuscript.

Categories and Subject Descriptors (according to ACM CCS): I.3.3 [Computer Graphics]: Picture/Image Generation—Digitizing and scanning

1. Introduction

Digital imaging has been highly successful in giving scholars access to the visual appearance of physical artifacts that they cannot access in person. Colorimetrically accurate images allow scholars to perform comparative studies of objects that are scattered around the world. Further, high quality images allow the general public to have access to the world's cultural treasures. However, imaging is capable of doing more than just visual reproduction. Digital imaging systems can be designed as measurement systems. Measurement systems can collect data that allow scholars to answer additional questions about artifacts that cannot be answered by means of simple visual inspection. These questions include, "What materials were used to form the artifact?" and "What sequence of changes were made in the artifact?". Measurement with digital imaging is appealing because it does not require the physical removal of material from the artifact. To use an imaging system for measurement, however, different choices for the optical components in the system are needed, as well as a different characterization of the performance of the system in terms of physical, rather than visual properties.

The efficiency of commercial cameras for visual reproduction is based on the trichromatic theory of human vision.

On a very simplified level, the human visual system (HVS) works by producing three signals resulting from visible light falling on three types of cone receptors in the retina. Camera sensors and filters are designed to approximate these three signals. A camera is characterized by a transformation (generally a three-by-three matrix) that converts the values produced by the sensor to a device independent coordinate system, such as CIEXYZ [Joh02]. Devices for visual production, such as computer displays, are similarly characterized, so that displayed images give a viewer the same visual impression as the original scene.

To use an imaging system as a measurement device for analysis, different sensors and filters are needed, as is a different characterization. Rather than just sensing visible light, it is useful to sense both ultraviolet and infrared radiation as well. Filters that are optimized for visual reproduction are poor for identifying the spectral wavelength distribution of light, so they need to be replaced with filters with well-defined spectral ranges. Rather than finding a transformation that converts the imaging output to an HVS-oriented standard color space [MJ02], we need a radiometric characterization that converts the output into the average radiance within well-defined spectral ranges.

Recently, a number of multispectral and hyperspectral imaging systems have been developed for measurement and documentation of artifacts [FK06]. These high-end systems have the disadvantages of high cost and/or long acquisition times. In this work, we show how measurements can be performed without such a high-end system based on the nature of the spectral properties of the artifacts in question. In particular, we consider the imaging of a medieval manuscript and identifying the pigments used. We show that a physically characterized system that captures data in five broad bands in the range of near-ultraviolet to near-infrared radiation can successfully identify pigments.

In the following sections we begin by briefly reviewing previous work in imaging artifacts. We then examine the key issues in the selection of components for an imaging system for measurement. We describe a method for both colorimetrically and radiometrically characterizing an imaging system. Finally, we present a case study in which a five-band, radiometrically characterized, imaging system is used for pigment identification in a medieval manuscript.

2. Background and Previous Work

This section describes the background and presents a brief discussion of previous techniques.

2.1. Spectral Imaging

Electromagnetic radiation can be captured physically by an optical mechanism. The electromagnetic radiations are commonly described in terms of the photon wavelengths. The spectral ranges can be classified into three big categories — near-ultraviolet (NUV): 300–400nm; visible (VIS): 400–700nm; near-infrared (NIR): 700nm–3.0μm [ISO07]. Trichromatic and multispectral imaging deals with VIS; hyperspectral imaging refers to NUV or NIR sensing, including VIS. In particular, many VIS/NIR imaging applications have been popular for painting pigment identifications in the conservation and cultural heritage contexts [FK06].

In practice, high-end hyperspectral imagers with narrow (e.g. 10nm) bands can cost in excess of €100,000, in contrast with high quality commodity cameras that are available for less than €2,000–4,000. In our work, we use a device in the middle ground—an imaging device designed for applications in astronomy, costing about €4,000. The device allows us to improve performance over a commodity camera by extending the detectable wavelength range that is sensed and allowing the use of filters with sharp wavelength cut-offs.

Spectral imaging can be categorized into two different designs. First, when a full-spectrum light source illuminates an object's surface, the reflected light is captured by a narrow bandpass filtered device [WCC*00, ACC*03, RB05]. The narrow bandpass filters on a motorized wheel or liquid crystal tunable filter (LCTF) are employed to discriminate the incident spectrum. Alternatively, a spectral dispersion unit can be used instead of bandpass filters. Spectral images are reconstructed through inverse solving, but it yields computational artifacts and a smaller spatial resolution than filter-banded imagers [KCWB10]. Second, a monochromatic sensor captures an object's surface, illuminated by a set of narrow-banded illuminations [EKCB*10, FCBTB10, KZD*10]. This method does not illuminate a subject with a full spectrum light source such as a Xenon light source; hence, it can minimize the ionization damage. Thanks to the evolution of LED technology, the configuration of narrow-banded LED lights would be more cost-efficient than the full spectrum light source; however, fluorescence (the emission of light by a substance that has absorbed light of a different wavelength such as NUV) are baked in the reflected light, interfering reflectance measurements of each wavelength.

2.2. Radiometry, Colorimetry, and Characterization

Radiometry refers to the measurement of optical radiation, which is an electromagnetic radiation within the frequency range of 3×10^{10} to 3×10^{16}Hz [CIE86]. In contrast, photometry is the measurement of light, which is defined as electromagnetic radiation detectable by the human eye within the wavelength range from 380nm to 780nm [CIE86]. Colorimetry is the measurement of human color perception, interpreting radiometric spectra to trichromatic human color perception. The Commission Internationale de l'Eclairage (CIE) defined the standard colorimetric observation, so-called color matching functions (CMFs) [CIE86] which defines psychophysically driven trichromatic cone responses within visible spectral range. The responsivity of modern trichromatic camera filters approximates that of these CMFs.

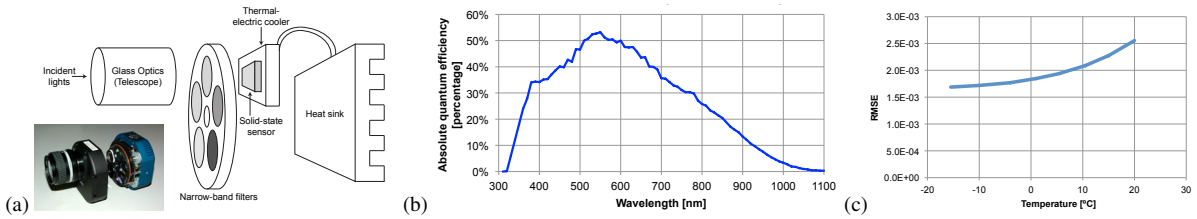

Figure 2: *(a) shows a typical configuration of an astronomical imager. (a) inset is the spectral imager that we employed. (b) Quantum efficiency of its semiconductor (Kodak KAF-8300). The spectral sensitivity of the sensor has a peak at 550nm and sensitivity spreads between 320 and 1100nm, covering from NUV to NIR. (c) compares RMS noise measurements at different sensor temperatures.*

CIEXYZ coordinates could be derived by taking the product of a light source $L(\lambda)$, a subject's reflectance $\rho(\lambda)$, and CMFs $\bar{x}(\lambda)$, $\bar{y}(\lambda)$, and $\bar{z}(\lambda)$:

$$\begin{aligned} X &= K_m \sum_{\lambda} L(\lambda)\rho(\lambda)\bar{x}(\lambda)\Delta\lambda \\ Y &= K_m \sum_{\lambda} L(\lambda)\rho(\lambda)\bar{y}(\lambda)\Delta\lambda \\ Z &= K_m \sum_{\lambda} L(\lambda)\rho(\lambda)\bar{z}(\lambda)\Delta\lambda, \end{aligned} \tag{1}$$

where K_m is the maximum photographic luminous efficacy 633lm/W. This Y value corresponds to luminance (unit: cd/m^2) [Hun98].

The trichromatic structure of colorimetry has been smoothly integrated into the trichromatic imaging system. Three different color filters (red/green/blue or cyan/magenta/yellow) are engraved on the semiconductor to mimic the CMF responsivity.

$$\begin{aligned} R &= \sum_{\lambda} L(\lambda)\rho(\lambda)D_r(\lambda)\Delta\lambda \\ G &= \sum_{\lambda} L(\lambda)\rho(\lambda)D_g(\lambda)\Delta\lambda \\ B &= \sum_{\lambda} L(\lambda)\rho(\lambda)D_b(\lambda)\Delta\lambda, \end{aligned} \tag{2}$$

where $D_{r/g/b}(\lambda)$ are spectral sensitivity of the three channels and $R/G/B$ are the trichromatic response values of a pixel on the sensor.

Assuming Grassmann's Additivity Law (any color can be matched by certain amounts of multiple primaries) [Hun98] and the linear response of the semiconductor to given electrons, we could drive a linear transform from $D_{r/g/b}(\lambda)$ to CMFs, since we have a sample population of pairs of XYZ and RGB in Eqs. (1) and (2). For instance, known reflectance measurements under certain illumination conditions (CIE D50 illuminant) [MJ02,Joh02,ISO06] or a transmittance target with illumination [KK08] are employed; or a monochromatic light source is used to derive full spectral sensitivity of the camera system [MVPC00, MVPC03, ISO06, NFG07].

Sugiura et al. [SKW*00] introduced a direct reconstruction method of reflectance by using a multispectral camera. Zhao and Berns [ZB07] proposed an approach for approximating reflectance from multispectral imaging, based on Wyszecki's metameric hypothesis. Zhao et al. [ZBTC08] demonstrated a pigment mapping application of multispectral imaging. Note that the development and validation of these methods were implemented assuming human color perception. In contrast, our application focuses on radiometric accuracy—exploiting NUV/VIS/NIR—as an extension of [SKW*00]. See Fig. 5(a) for an example of measured spectral sensitivity of a trichromatic camera. Our characterization takes a mixed approach by using radiance measurements of reflective samples with a full spectrum light source of NUV/VIS/NIR.

2.3. Application – Manuscript Analysis

We demonstrate the use of a characterized imaging system in the analysis of a medieval manuscript written by the English scholar John Gower in the 15th century. The manuscript was written in old English and French for main texts, and Latin for rubric summaries. The text of the manuscript is the third recension of the Confessio Amantis. Also contained are some Latin and French poems. This manuscript had been in a family's possession for a century (see Fig. 6(d) for the mildew damage). While their house was almost destroyed by a fire in the 18th century, the manuscript became damp and damaged by mildew.

Paleographic study on this manuscript suggests that red lead, brazilwood, cochineal, dragon's blood, azurite, and iron gall ink might have been used for lettering. Identifying the original pigments is challenging and a number of scientific techniques have been tried [Cla01]. The spectral reflectance of the candidate pigments is shown in Fig. 11. The smooth variation of reflectance with wavelength allows us to use a relatively small number of wavelength bands to differentiate between the pigments.

3. Optics – Selection and Characterization

In this section, we discuss the selection of the optics that allow imaging from NUV to NIR. We also describe the characterization of the system that allows us to transform the output from the imaging system into average radiance values in well-defined wavelength bands.

3.1. Solid-State Sensor

Our goal in this hardware configuration is to build a compact and mobile spectral imaging system, which covers NUV/VIS/NIR spectra. We chose an astronomical imaging system equipped with a Kodak KAF-8300 sensor (with

micro-lens) with a built-in motorized filter wheel (QSI 583). See Fig. 2 for the structure of our employed imager and the quantum efficiency of the semiconductor [Kod08]. Its quantum efficiency covers a spectrum from 320 and 1100nm. It is enough for sensing our target range of NUV through NIR for our application.

Temperature Like the other astronomical imagers, this imager includes thermal-electric (TE) cooling, so-called Peltier cooling. While a camera is operated, thermally produced electrons accumulate in the pixels, which interfere with the electrons (converted from the captured photons) that make up the image. For instance, when the shutter is opened for 30 seconds to take a NUV shot, the sensor temperature increased in 1∼2°C. This accumulation of the thermal electrons is called *dark current noise*. This lowers the dynamic range of the sensor and accordingly reduces the signal-to-noise ratio. We keep the temperature of the image below approx. -15°C for capturing images, which requires about 3-4 minutes preparation time when the camera boots up. In particular, this cooling is beneficial when capturing NUV with ordinary glass optics. Fig. 2(c) compares measured RMS noise at different temperatures.

3.2. Lens

Our objective of this design is to cover the continuous spectral range from NUV to NIR. We first characterized the spectral transmittance of two different types of lenses: (a) glass-based Nikon (24mm F2.8) and (b) quartz-based Jenoptik CoastalOpt (60mm F4). Fig. 3 compares the differences of transmittances of these two lenses—in particular transmittance of NUV and NIR—measured by a calibrated spectrometer (Ocean Optics USB2000). The NUV transmittance of the Nikon lens drops down rapidly from 430nm and NIR transmittance starts to decrease from 770nm. This lens provides even spectral transmittance from 430nm to 770nm. In contrast, the Jenoptic lens shows steady transmittance from 400nm to 850nm. This quartz-base lens appears relatively more efficient in transmitting NUV than the glass-based optics.

Fig. 5 shows complete spectral sensitivities with two different optics. The quartz-based lens appears optimal for NUV/VIS/NIR; the glass-based lens could be a better choice for VIS/NIR. The respective lens should be selected for a particular target spectral range. Our filter configuration with the Nikon lens can capture isolated NUV (370–400nm) and NIR (660–900nm) with Peltier cooling. We chose this optics for our manuscript imaging, considering the focal length of the optics and cost efficiency.

3.3. Imager Characterization

We employed five bandpass filters: Astrodon UV and Baader Blue/Green/Red/IR filters. Their hyperspectral transmittances were measured with an oxygen-free Xenon light source (5495 K). Fig. 4 presents the transmittance measurements.

In Eq. (2), the spectral sensitivity of the camera $D(\lambda)$ is the product of quantum efficiency of the semiconductor $Q(\lambda)$ and filter transmittance $T_{1,2,\ldots,n}(\lambda)$. Assuming we have n filters, the raw camera responses $C_{1,2,\ldots,n}(\lambda)$ of each channel are:

$$\begin{aligned} C_1 &= \sum_{\lambda} L(\lambda)\rho(\lambda)Q(\lambda)T_1(\lambda)\Delta\lambda \\ C_2 &= \sum_{\lambda} L(\lambda)\rho(\lambda)Q(\lambda)T_2(\lambda)\Delta\lambda \\ &\vdots \qquad\qquad \vdots \\ C_n &= \sum_{\lambda} L(\lambda)\rho(\lambda)Q(\lambda)T_n(\lambda)\Delta\lambda. \end{aligned} \tag{3}$$

By averaging the radiance measurements $L(\lambda)\rho(\lambda)$ of n filter bandwidths, we can compute multi-band radiance measurements $\overline{\Psi}_{1,2,\ldots,n}$.

$$\begin{aligned} \overline{\Psi}_1 &= \tfrac{1}{|\lambda_1|}\sum_{\lambda_1} L(\lambda_1)\rho(\lambda_1)\Delta\lambda_1 \\ \overline{\Psi}_2 &= \tfrac{1}{|\lambda_2|}\sum_{\lambda_2} L(\lambda_2)\rho(\lambda_2)\Delta\lambda_2 \\ &\vdots \qquad\qquad \vdots \\ \overline{\Psi}_n &= \tfrac{1}{|\lambda_n|}\sum_{\lambda_n} L(\lambda_n)\rho(\lambda_n)\Delta\lambda_n, \end{aligned} \tag{4}$$

where $|\lambda_{1,2,\ldots,n}|$ is the cardinality of $\lambda_{1,2,\ldots,n}$. Once we have two data sets—the full spectral camera signals $\mathbf{C}$ and the radiances $\overline{\mathbf{\Psi}}$ from a number of training samples (see Fig. 7(a))—we derive a linear affine transform $\mathbf{M}$ by solving: $\mathbf{M} = (\mathbf{C}^\top\mathbf{C})^{-1}\mathbf{C}^\top\overline{\mathbf{\Psi}}$. Ordinary camera characterization models (with respect to human color vision) map camera signals in Eq. (2) into CIEXYZs in Eq. (1); however, they introduce a metameric limitation in identifying reflectance. In contrast, our characterization model transforms the n-channel camera signals $C_{1,2,\ldots,n}$ in Eq. (3) directly into the multi-band radiance measurements $\overline{\Psi}_{1,2,\ldots,n}$ in Eq. (4). This method provides more discrimination power than CIEXYZ-

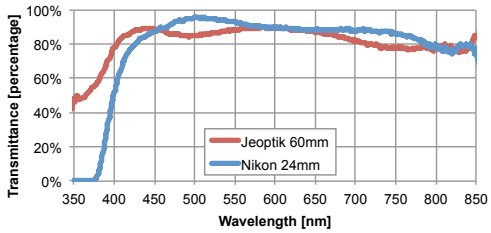

Figure 3: *Measured transmittance of a quartz-based (Jeoptik CoastalOpt 60mm) and a glass-based (Nikon 24mm) lenses.*

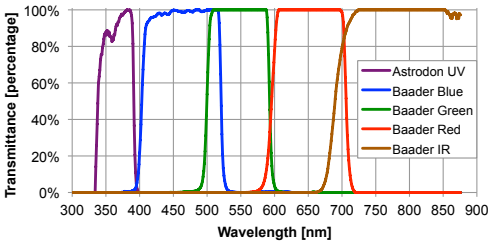

Figure 4: *Measured transmittances of our five bandpass filters.*

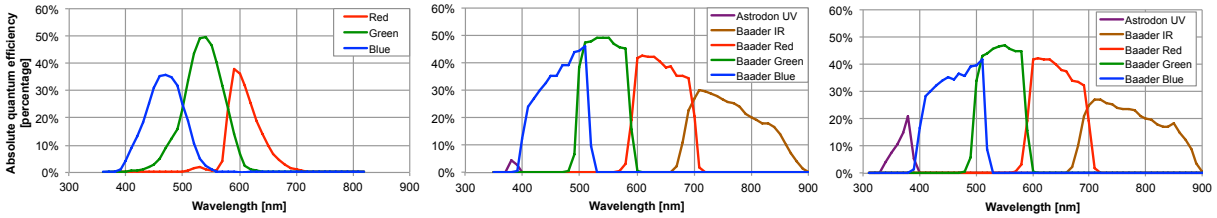

(a) *Ordinary RGB camera* **(b)** *Hyperspectral camera with a glass optics* **(c)** *Hyperspectral camera with a quartz optics*

Figure 5: *(a) Spectral sensitivity of an ordinary RGB camera (Nikon D70). Each trichromatic filter has a 200–300nm band width from 380nm and 700nm. Note that the entire blue channel overlaps with the green channel and that half of the red channel overlaps with the green channel. (b) Spectral responsivity of our spectral imager with the five narrower-band filters through a glass-based optics (Nikon 24mm). Note that the NUV responsivity of the system is smaller than other bandwidths. (c) Spectral responsivity of our system with a quartz lens (Jenoptik CoastalOpt 60mm). The NUV responsivity increases significantly, but the NIR responsivity is limited to 900nm.*

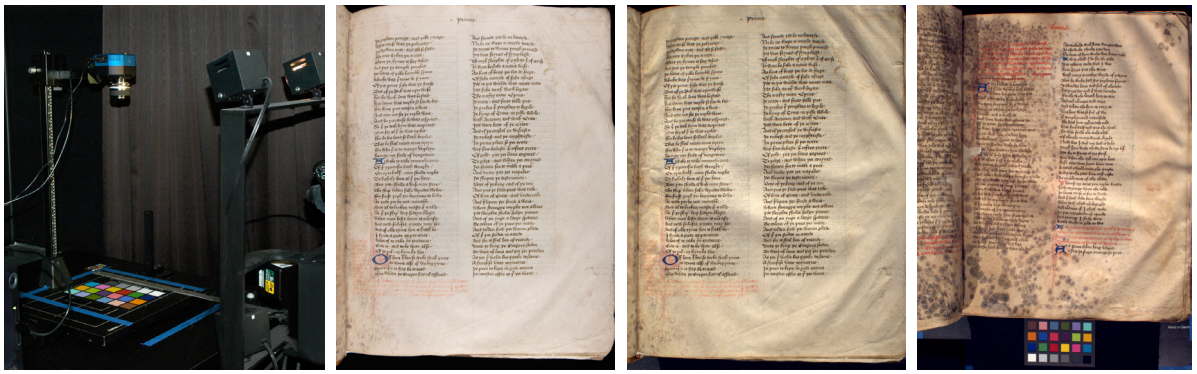

(a) *Experimental setup* **(b)** *A trichromatic camera* **(c)** *Our method (6 recto)* **(d)** *Our method (53 recto)*

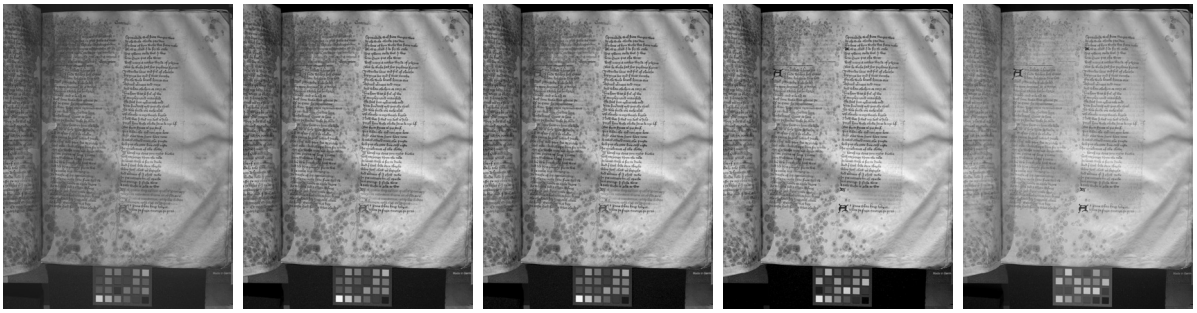

(e) *380nm (370–390nm)* **(f)** *455nm (390–520nm)* **(g)** *535nm (480–590nm)* **(h)** *640nm (570–710nm)* **(i)** *800nm (660–900nm)*

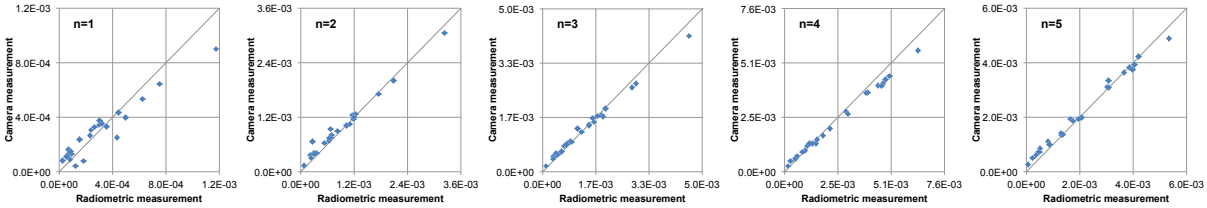

(j) *380nm (370–390nm)* **(k)** *455nm (390–520nm)* **(l)** *535nm (480–590nm)* **(m)** *640nm (570–710nm)* **(n)** *800nm (660–900nm)*

Figure 6: *Image (a) shows our experimental setup. Image (b) of page 6 recto was captured by a high-end trichromatic digital camera (Canon EOS-1Ds Mark III). The Latin rubric appears too faint. Image (c) of the same page that was captured by our characterized imaging system. The rubric appears clearer in this capture. Image (d) of 53 recto in the same manuscript shows an seriously damaged by mildew. Reflectances are measured by our characterization method. Images (e)–(i) present captured radiances. These images are rendered by normalizing the computed radiance map into the display signals through gamma correction. Plots (j)–(n) show the accuracy of each filter bandwidth between our image-based measurements and radiometric measurements. Ideally the scattered dots would be on a diagonal line.*

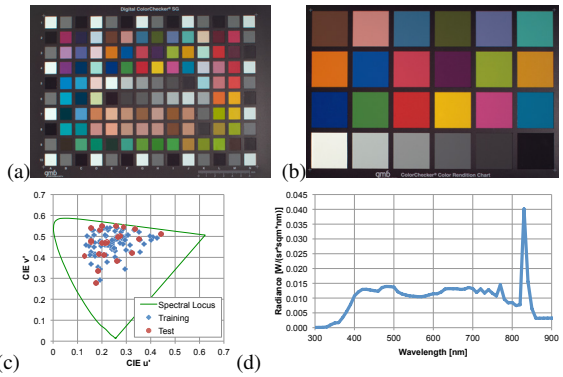

Figure 7: *(a) and (b) show the employed training (140 colors) and test (24) color samples. (c) compares the gamut differences of the targets. (d) is the spectral measurements of our Xenon light source.*

based characterization. The characterization process yields $\mathbf{M}$ from the training data; we then estimate the radiances by computing: $\overline{\mathbf{\Psi}} = \mathbf{CM}$.

Fig. 7 shows the color targets under the full-spectrum light source. (a) is for training, and (b) is for testing. (c) compares gamut distributions of the two targets. (d) shows the measured spectral power distribution of the employed Xenon light source. Note that this light source covers the spectral range from 300 to 900nm.

Testing Variation We evaluated the qualitative difference by finding the coefficient of variation (CV). Suppose there are two different data sets x and y. The calculation of CV is:

$$\mathrm{CV} = \frac{100}{\bar{y}} \sqrt{\frac{1}{N}\sum_i (x_i - y_i)^2},$$

where $\bar{y}$ is the mean of the data set y and N is the number of y elements. The deviation in this CV is calculated from the difference between two elements $(x_i - y_i)$, similar to RMS error, which is then normalized by the mean in a percentage scale.

4. Results

We characterized our imaging system both colorimetrically and radiometrically, and compared the characterization to results using commodity cameras. Fig. 8(a) shows the results of a classical colorimetric characterization that relates camera output to CIEXYZ values [ISO06]. We employed RAW outputs of the commodity cameras by interpolating bayer-pattern signals into three channels. Three-by-three linear transforms for each camera were derived from the training color samples and were then evaluated using a new test scene under a different illumination. Our imaging system performs in the same range as the commodity cameras with respect to color accuracy.

Fig. 8(b) shows the results of radiometrically characterizing the systems. The plots show the accuracy of the average radiance value given by each system, for the wavelength bands in which each channel has non-zero sensitivity. Note that the commodity cameras have much larger bands (200–300nm) than our imager (100–150nm). See Fig. 5. The results in Fig. 8(b) show that the commodity cameras have much higher error in estimating average radiance over less localized wavelength bands. This effect is further diagrammed in Fig. 9. An ideal system would be in the lower left-hand corner of this figure – it would give results with no error over wavelength bands of vanishingly small width. Because our imager has a small number of bands, the bandwidth is larger than the ideal. However, the wavelength range is better defined for the results of our imaging system than for the commodity cameras, and the estimated average radiances are more accurate.

Fig. 6 presents visual production of the manuscript, captured with our method by converting CIEXYZ coordinates into sRGB display signals. Compared with an ordinary trichromatic camera capture (b), our capture (c) not only pro-

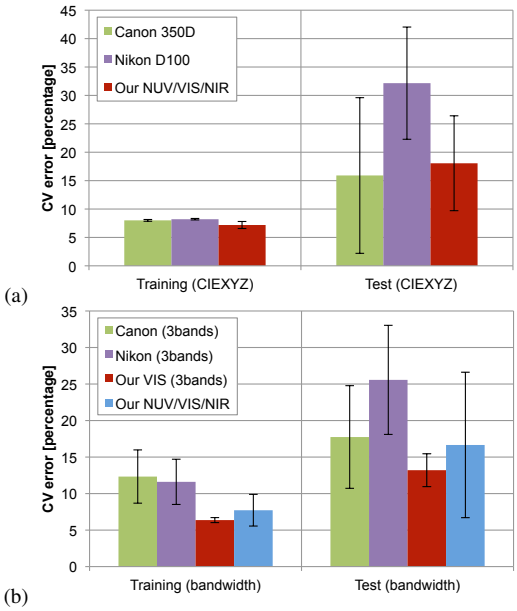

Figure 8: *Average accuracy of characterization. Our NUV/VIS/NIR imager is compared with Canon 350D and Nikon D100. The training presents the predicted color accuracy with the training data (140 patches under the Xenon lamp). The test shows the accuracy with a different test data set (24 patches under a halogen lamp with an NIR-blocking filter). A side of the error bar represents the standard deviation of bands or XYZ channels.*

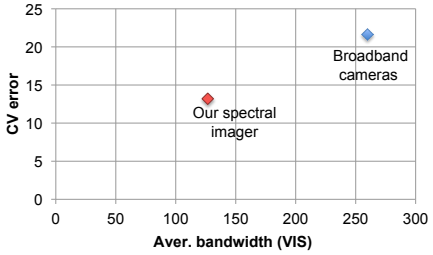

Figure 9: *Bandwidth vs. radiometric accuracy.*

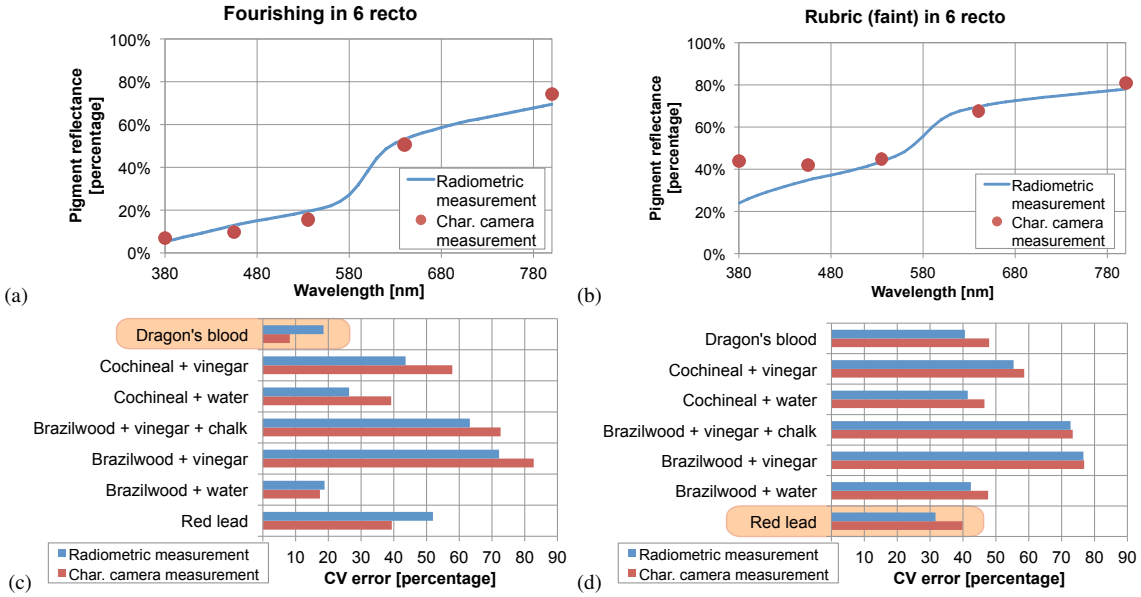

Figure 10: *(a) and (b) show the reflectance of the target pigments, measured by our method and a spectrophotometer. (c) and (d) present the result of pigment identification, determined by testing CV errors between the measured reflectance with candidate reflectances. Both instruments identify the English flourishing as Dragon's blood and the washed-out rubrics as Red lead. R^2 of the two instruments is 0.9240.*

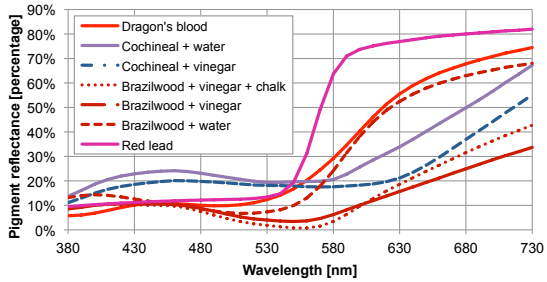

Figure 11: *Measured reflectance of red candidate pigments.*

vides sharper color discrimination, but also captures NUV (aver. 380nm in a range of 370-390nm) and NIR (aver. 800nm in a range of 660-900nm). See Images (e)–(i). Plots (j)–(n) show accuracy of the predicted radiance in each bandwidth under the same light source, corresponding to (e)–(i).

5. Pigment Identification

The objective of our radiometric characterization is to use our imaging system as a measuring tool rather than merely for making a visual production. We used our imager to assist textual pigment identification in the medieval manuscript. In particular, we were interested in two red pigments: one for flourishing, and the other one for rubricating in 6 recto (see Fig. 1 for measured points).

Prior to our imaging analysis, we built a reflectance gallery of seven candidate pigments on a parchment (same as the manuscript—but modern), which are particularly red and were popular for rubrication in the 15th century [Cla01], by measuring reflectances with a spectrophotometer (GretagMecbeth EyeOne): Red lead (lead tetroxide, Pb_3O_4), Brazilwood (Redwood–brazilin, red colorant in wood, $C_{16}H_{14}O_5$) with water, Brazilwood with vinegar, Brazilwood with vinegar and chalk, Cochineal (cochenille–carminic acid, $C_{22}H_{20}O_{13}$) with water, Cochineal with vinegar, and Dragon's blood ink.

Our characterized imager measures the incident radiance $R_{1,2,...,5}$ with 5 bandwidths. Defining $L(\lambda_1), L(\lambda_2), ..., L(\lambda_5)$ and $\rho(\lambda_1), \rho(\lambda_2), ..., \rho(\lambda_5)$ in Eq. (4) as $L_{1,2,...,5}$ and $\rho_{1,2,...,5}$, in order to derive the reflectance of the captured pigment $\rho_{1,2,...,5}$ from $R_{1,2,...,5}$, we need the irradiance measurements of the light source $L_{1,2,...,5}$. To do that, we employed a material with known and even spectral reflectance such as the ColorChecker patch A4 or Spectralon. Then, the captured reflectances $\rho_{1,2,...,5}$ are driven by: $\rho_1 = R_1/L_1$, $\rho_2 = R_2/L_2$, ..., $\rho_5 = R_5/L_5$. See Fig. 10(a) and (b) for our camera measurements of the flourishing and the rubric samples.

We test the coefficient of variation of our characterized camera measurements with a dense number of spectral samples measured on the manuscript with a spectrophotometer. The values given at the center of the wavelength bands for our characterized system match well with the spectrophotometer results. The advantage of our imaging system is that we can gather data on a full manuscript page rather than at the isolated points that we can measure with the spectroradiometer.

6. Discussion

Currently, we configured our system with a minimal number of filter bands. The radiances of each band were calculated

by averaging radiances within each bandwidth. As shown in Section 5, the low-frequency reflectance properties of the textual pigments could be well identified with high accuracy. As future work, we intend to investigate higher frequency reflectances with narrower bandpass filters such as LCTF, in order to reduce metameric errors.

One optical issue in focusing was noticed when the Nikon lens was used for NUV and NIR imaging. This lens' focal length is designed for VIS, and the spectral dispersion of NUR/NIR requires adjustments of the focal length. An small image size differences of NUV and NIR were manually adjusted to register them with other VIS channels.

Our pigment identification is based on the maximum likelihood of the measured reflectance on the same parchment substrate. Our current analysis does not include the *Kubelka-Munk* theory [Mac97]. Testing our system performance with different pigments and substrates, compared with costly x-ray reflectrographic measurements as ground truth, would be an interesting future direction.

6.1. Conclusions

In this paper, we discusses the practical selection and radiometric characterization for a bandpass-filter imaging system. Our appropriately selected optics and characterization approach allow us to measure NUV, VIS, and NIR radiance as a function of wavelength. We demonstrate that our system can be used for pigment identification in a manuscript. The results validate the accuracy in identifying the pigments, rivaling the performance of a spectrophotometer.

Acknowledgements

We would like to thank Marie-France Lemay for preparing pigment samples and Barbara Shailor for her paleographic comments on the manuscript.

References

[ACC*03] ATTAS M., CLOUTIS E., COLLINS C., GOLTZ D., MAJZELS C., MANSFIELD J., MANTSCH H.: Near-infrared spectroscopic imaging in art conservation: investigation of drawing constituents. *Journal of Cultural Heritage 4* (2003), 127ÃŘ–136. 2

[CIE86] CIE: *Colorimetry*. Publication CIE 15.2-1986, Commission Internationale de l'Eclairage (CIE), Vienna, 1986. 2

[Cla01] CLARKE M.: The analysis of medieval European manuscripts. *Reviews in conservation* (2001). Ancient pigment analysis. 3, 7

[EKCB*10] EASTON R., KNOX K., CHRISTENS-BARRY W., BOYDSTON K., TOTH M., EMERY D., NOEL W.: Standardized system for multispectral imaging of palimpsests. In *Proc. the SPIE, Computer Vision and Image Analysis of Art* (2010), no. 75310D, pp. 1–11. 2

[FCBTB10] FRANCE F. G., CHRISTENS-BARRY W., TOTH M. B., BOYDSTON K.: Advanced image analysis for the preservation of cultural heritage. In *Proc. SPIE 7531* (2010), no. 75310E, pp. 1–11. 2

[FK06] FISCHER C., KAKOULLI I.: Multispectral and hyperspectral imaging technologies in conservation: current research and potential applications. *Reviews in Conservation 7* (2006), 3–16. 2

[Hun98] HUNT R. W. G.: *Measuring Colour*, 3rd ed. Fountain Press, Kingston-upon-Thames, 1998. 3

[ISO06] ISO: *ISO/17321-1:2006: Graphic technology and photography — Colour characterisation of digital still cameras (DSCs) — Part 1: Stimuli, metrology and test procedures*. 2006. 3, 6

[ISO07] ISO: *ISO/20473:2007: Optics and photonics — Spectral bands*. 2007. 2

[Joh02] JOHNSON T.: Methods for characterizing colour scanners and digital cameras. In *Colour Engineering*, Green P., MacDonald L., (Eds.). John Wiley, Chichester, 2002, pp. 165–178. 2, 3

[KCWB10] KITTLE D., CHOI K., WAGADARIKAR A., BRADY D. J.: Multiframe image estimation for coded aperture snapshot spectral imagers. *Appl. Opt. 49*, 36 (2010), 6824–6833. 2

[KK08] KIM M. H., KAUTZ J.: Characterization for high dynamic range imaging. *Computer Graphics Forum (Proc. EUROGRAPHICS '08) 27*, 2 (2008), 691–697. 3

[Kod08] KODAK: Device Performance Specification: Kodak KAF-8300 Image Sensor. Revision 5.2 MTD/PS-0996, 2008. 4

[KZD*10] KIM S. J., ZHUO S., DENG F., FU C.-W., BROWN M.: Interactive visualization of hyperspectral images of historical documents. *IEEE Trans. Visualization and Computer Graphics 16*, 6 (nov.-dec. 2010), 1441 –1448. 2

[Mac97] MACDONALD L. W.: Colour in visual display. In *Colour Physics for Industry*, McDonald R., (Ed.), 2nd ed. Soc. Dyers Col., Bradford, 1997, pp. 373–425. 8

[MJ02] MACDONALD L., JI W.: Colour characterisation of a high-resolution digital camera. In *Proc. IS&T CGIV* (2002), vol. 1, pp. 433–437. 2, 3

[MVPC00] MARTÍNEZ-VERDÚ F., PUJOL J., CAPILLA P.: Calculation of the color-matching functions of digital cameras from their complete spectral responsitivities. In *Proc. CIC* (Nov. 2000), pp. 211–216. 3

[MVPC03] MARTINEZ-VERDU F., PUJOL J., CAPILLA P.: Characterization of a digital camera as an absolute tristimulus colorimeter. *J. IS&T 47*, 4 (2003), 279–374. 3

[NFG07] NORMAND C., FORNARO P., GSCHWIND R.: Automated digital camera sensor characterization. In *SPIE/IS&T EI* (2007), vol. 6502. 3

[RB05] RAPANTZIKOS K., BALAS C.: Hyperspectral imaging: potential in non-destructive analysis of palimpsests. In *Image Processing, 2005. ICIP 2005. IEEE International Conference on* (sept. 2005), vol. 2, pp. II – 618–21. 2

[SKW*00] SUGIURA H., KUNO T., WATANABE N., MATOBA N., HAYASHI J., MIYATA Y.: Development of a multispectral camera system. In *Proc. SPIE 3965 on Sensors and Camera Systems for Scientific, Industrial and Digital Photographic Applications* (Bellinghan, WA, 2000), SPIE, pp. 331–339. 3

[WCC*00] WARE G., CHABRIES D., CHRISTIANSEN R., BRADY J., MARTIN C.: Multispectral analysis of ancient maya pigments: implications for the naj tunich corpus. *IEEE Transactions* (2000), 2489–2491. 2

[ZB07] ZHAO Y., BERNS R. S.: Image-based spectral reflectance reconstruction using the matrix R method. *Color Research & Application 32*, 5 (2007), 343–351. 3

[ZBTC08] ZHAO Y., BERNS R. S., TAPLIN L. A., CODDINGTON J.: An investigation of multispectral imaging for the mapping of pigments in paintings. *SPIE 6810*, 681007-9 (2008). 3